Supplementary Information (SI) for EES Batteries.

Supplementary Information

Small Changes, Big Gains: Standardizing Non-Electrode Coin Cell Components in Aqueous Zinc Battery Research

Saptarshi Paul[a,Γ], James H. Nguyen[a,Γ], Michael L. Harrigan[a], Ashutosh Rana[a], Andy Berbille[a] and Jeffrey E. Dick[a,b*]

[a] Department of Chemistry, Purdue University, West Lafayette, IN, 47907, USA
[b] Elmore Family School of Electrical and Computer Engineering, Purdue University, West Lafayette, IN, 47907, USA

Γ: Denotes equal contribution

Corresponding Author
Jeffrey E. Dick (jdick@purdue.edu)

Experimental Section

Materials:
Zinc Sulfate (ZnSO4, high-quality reagent) was acquired from Sigma Aldrich. Zinc foil (99.9% purity) was purchased from MTI corporation. The chemicals were employed without the need for further purification. Deionized (DI) water was supplied by a Milli-Q ultrapure water generation system and was employed in the formulation of all aqueous electrolytes. Cu, Ti, Ni and SS foils were acquired from Goodfellow Advanced Materials. The separators were bought from sigma aldrich and were of thickness 0.15 mm.

Electrochemical Measurements:
All electrochemical tests were performed using a CHI6284 electrochemical workstation. CV and LSV measurements were conducted in a three-electrode set up as discussed in the main manuscript. CR2032 coin-type cells were assembled under ambient air conditions and assessed using a Neware battery test system. All electrochemical tests were conducted at 25 °C without specific conditions.

Material Characterization:
The FESEM was done using field emission scanning electron microscopy (FESEM, JEOL JSM-7500F). Aztec Oxford Instruments were used for EDX analysis. Phase structure exploration was carried out by XRD (Bruker D8 advanced) with Cu Kα radiation over the 5° to 60° 2 theta range.

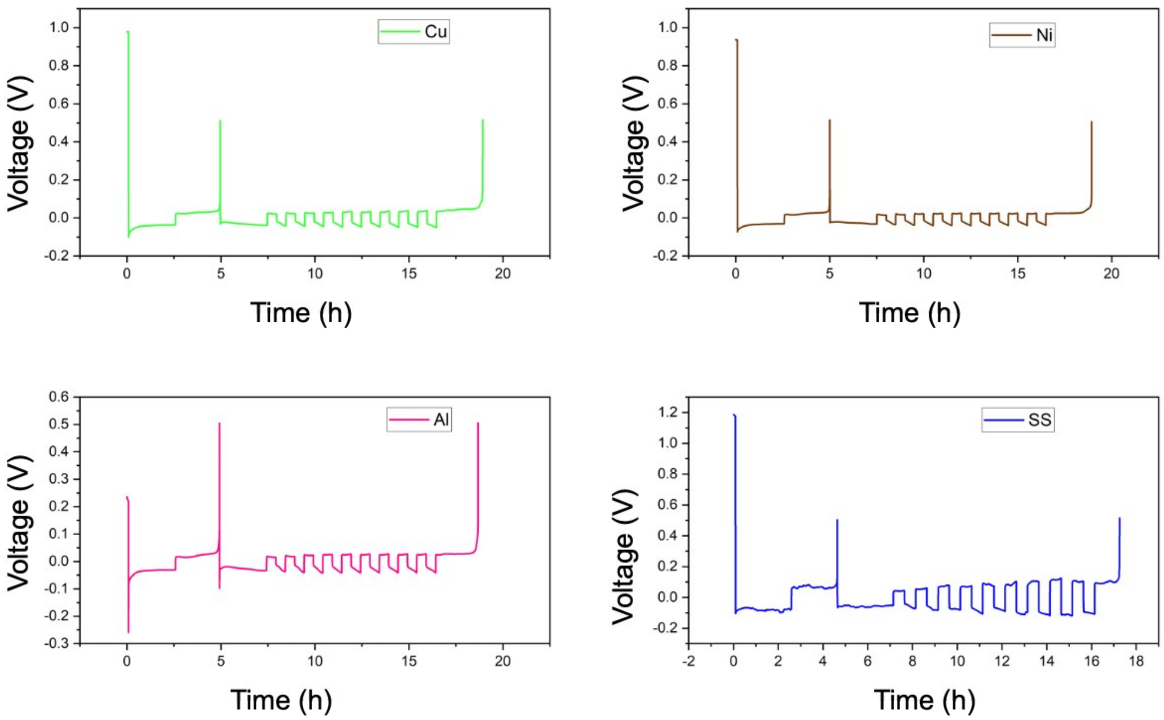

Fig. S1. The potential versus time curves for all the different current collectors under the galvanostatic charge-discharge protocol.

From the galvanostatic charge-discharge protocol (Aurbach), we get to see the better performance of Cu and Ti compared to Ni and SS as we extract the Coulombic Efficiency from these data.

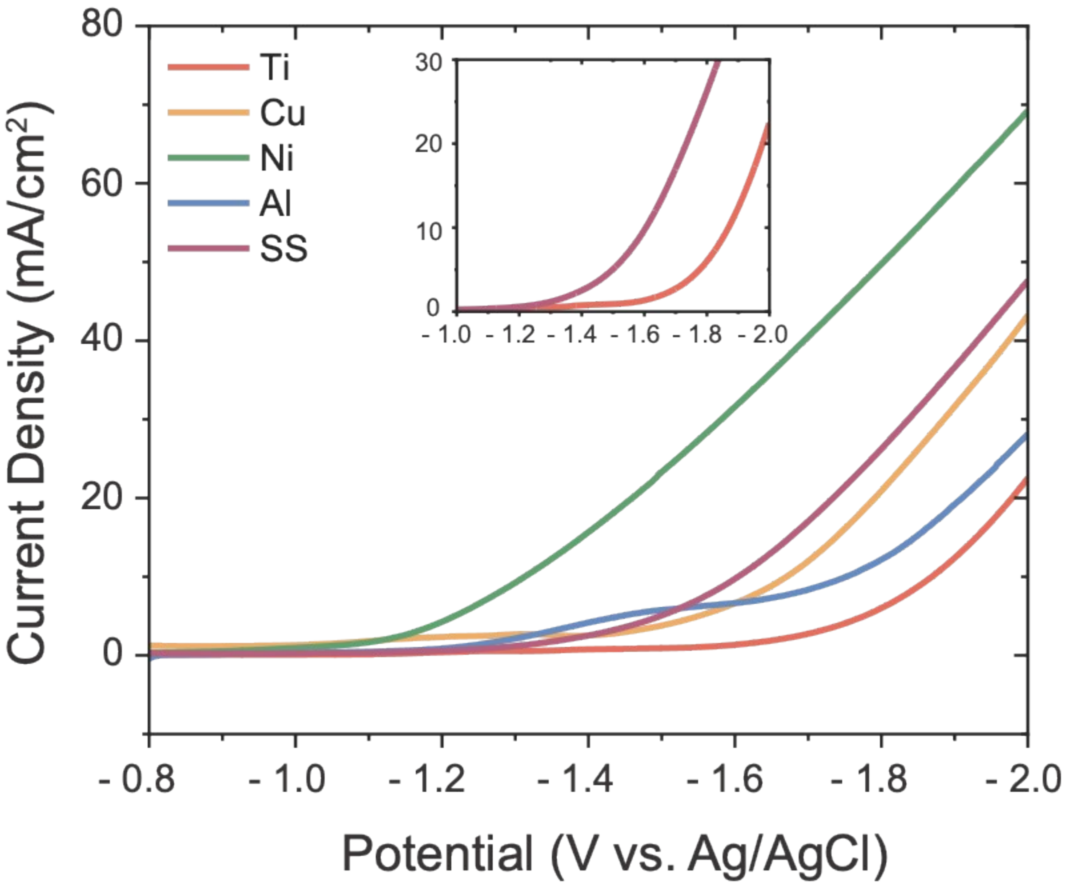

Fig. S2. The onset of hydrogen evolution reaction (HER) for the different current collector materials. The inset shows the difference in the onset of HER for Ti and SS.

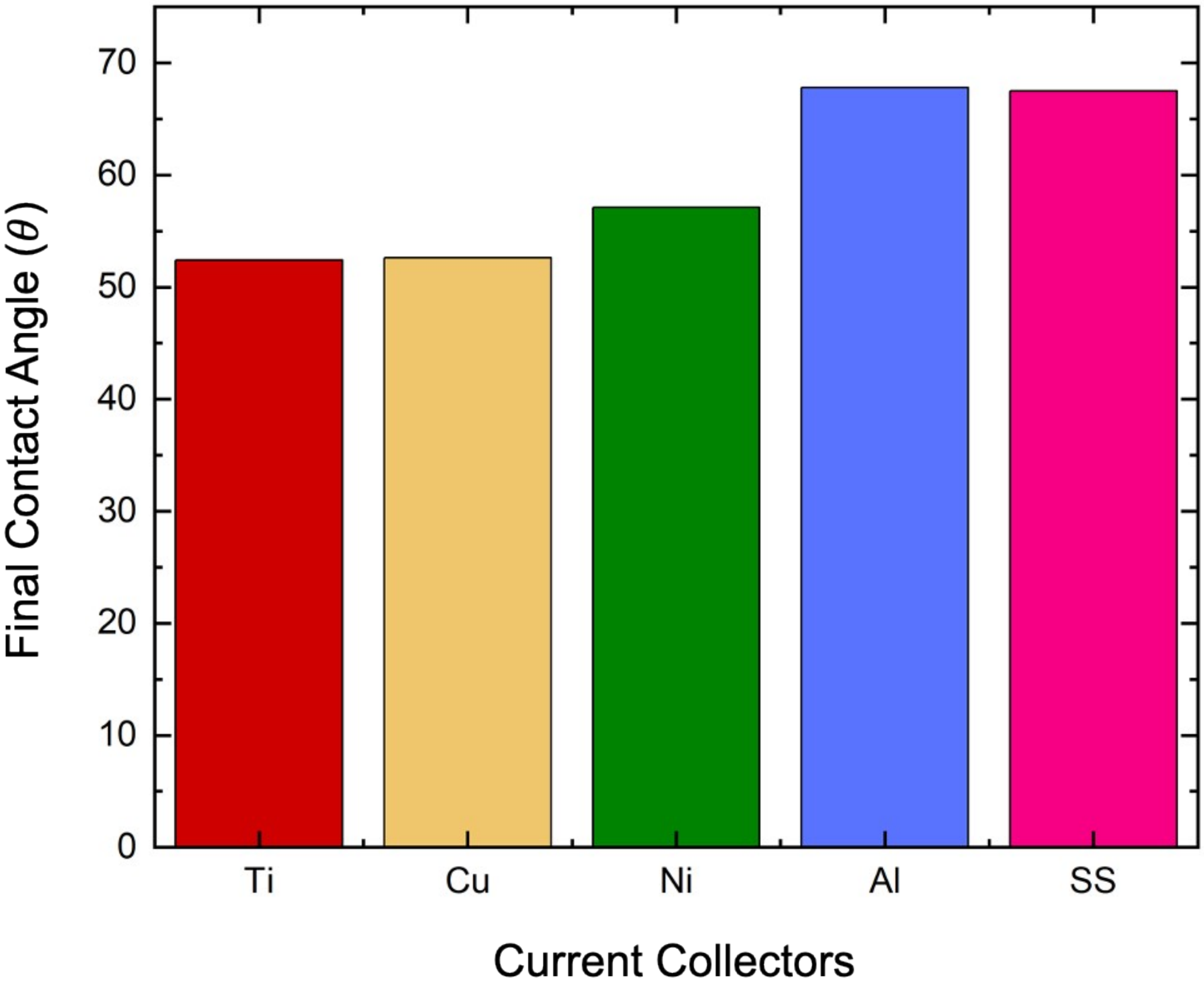

Fig. S3(A). Final contact angle measurements showing the contact angle after 10 minutes for the different current collectors.

We get to see different measurements in the contact angle for Ti and Cu, indicating more wettability and uniform deposition

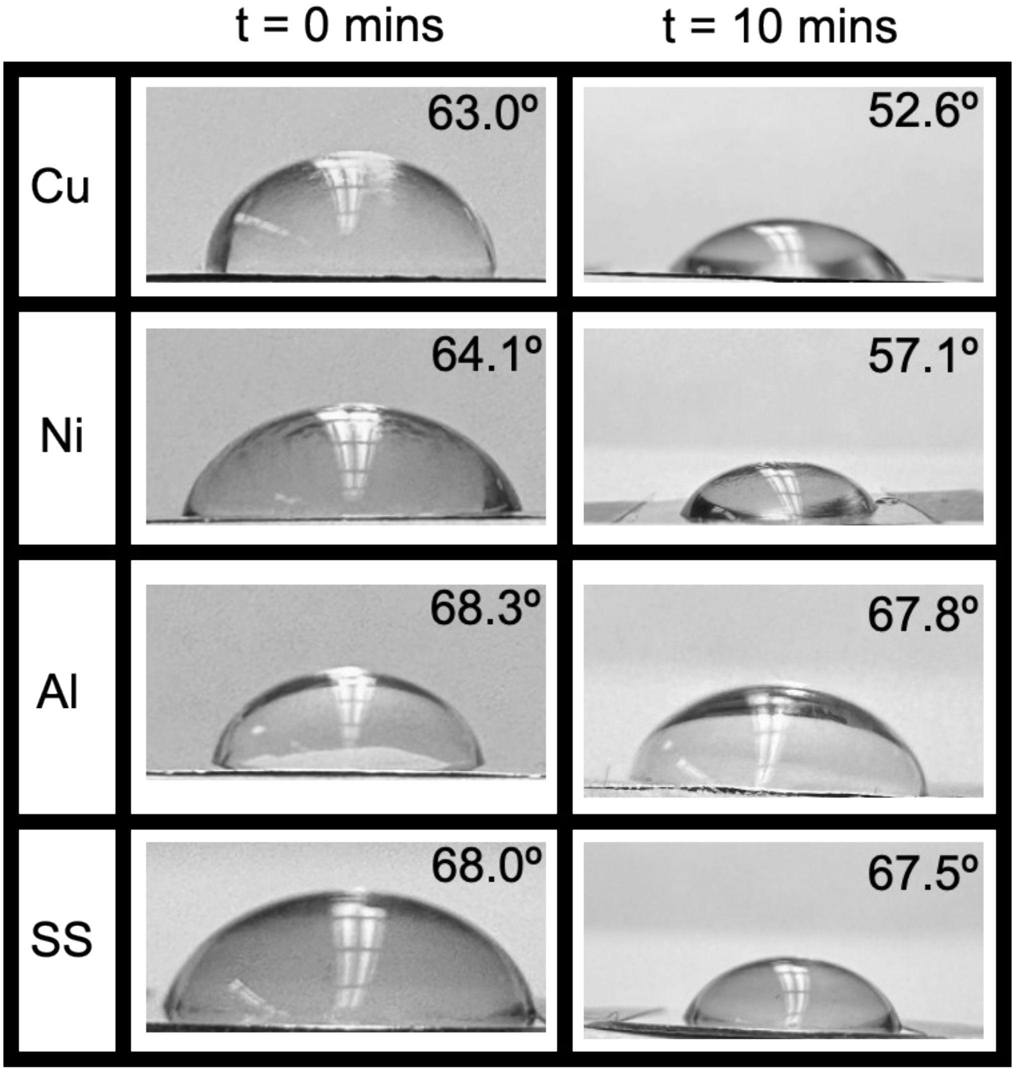

Fig. S3(B). Contact Angle measurements showing the difference in the contact angle after 10 minutes for the different current collectors.

Ti was already shown in the main figure. We get to see a big change in the contact angle for Ti and Cu, indicating more wettability and uniform deposition

Table S1. Intensity ratios of XRD peaks for all current collectors

Current Collectors	**$R_{002}/(R_{100} + R_{101} + R_{002})$**
Ti	0.583
Cu	NA
Ni	0.510
Al	0.357
SS	0.308

Current Collectors	**R_{002}/R_{100}**
Ti	4.63
Cu	4.07
Ni	0.832
Al	0.0414
SS	1.10

The higher ratio for the case of Ti and Cu indicates more planar orientations of Zn leading to homogenous deposition contributed via 002 facet. On the other hand, an excess of 100 facet indicates the presence of dendritic structures in the case of Ni and SS.

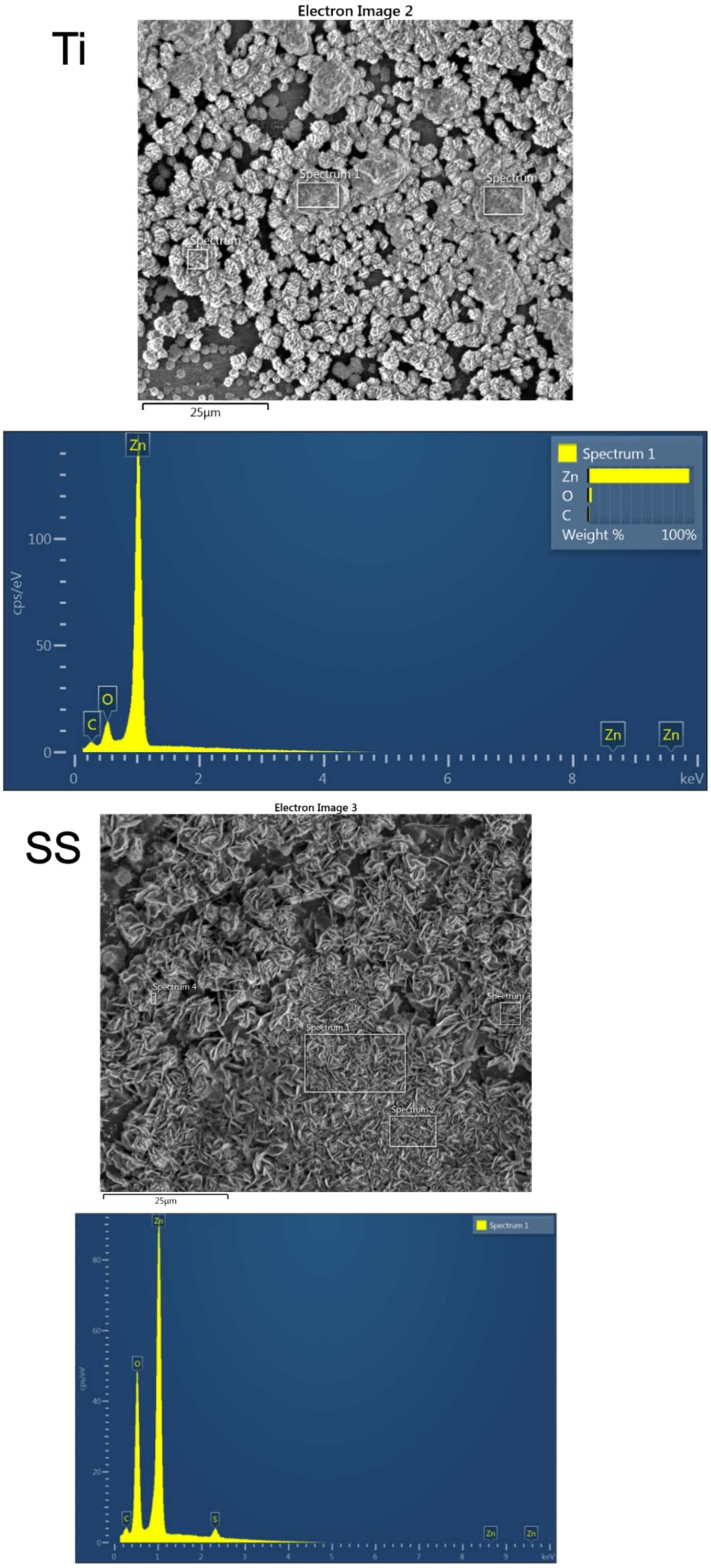

Fig. S4. SEM-EDX mapping for both Ti and SS after deposition.

EDX peaks showing the presence of sulfur with respect to Zn in case of SS, but not Ti.

Fig.S5. The thickness of a Zn||Cu half-cell after 50 cycles.

It is noted here that the thickness is even lower than the one for Ti, indicating lower HER generation and lower side products.

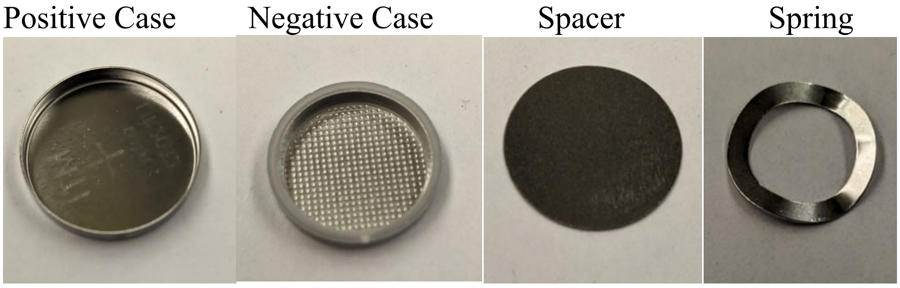

Positive Case

Negative Case

Spacer

Spring

Fig. S6. Fresh case, spacer, and spring before cycling

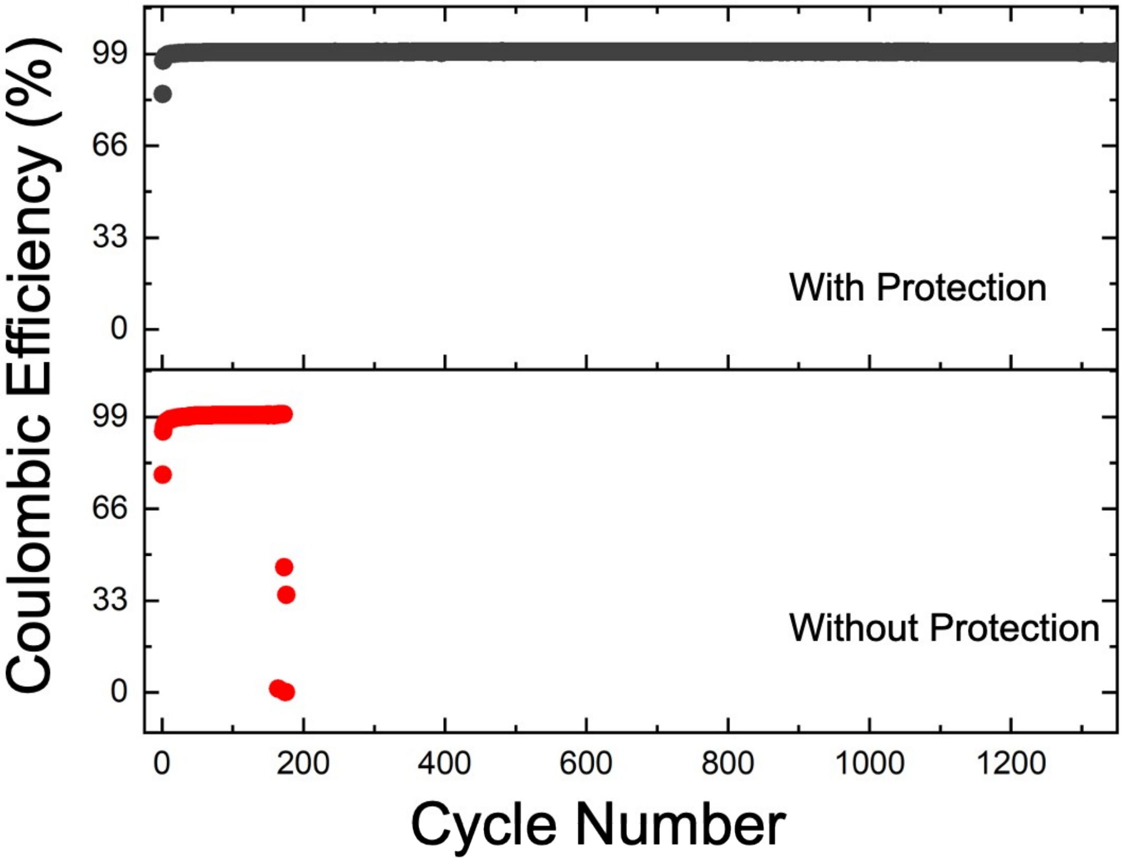

Fig. S7. The performance of a Zn||Cu cell with and without protection.

The coin cell without protection starts fluctuating around 50 cycles and is totally dead before it reaches 200 cycles, whereas the one with protection crossed 1000 cycles.

Fig. S8. The potential versus time curves for Zn-Cu half-cells without protection under the galvanostatic charge-discharge protocol (Aurbach).

It was found that the Coulombic Efficiency from here was lower than the obtained with the protection included.

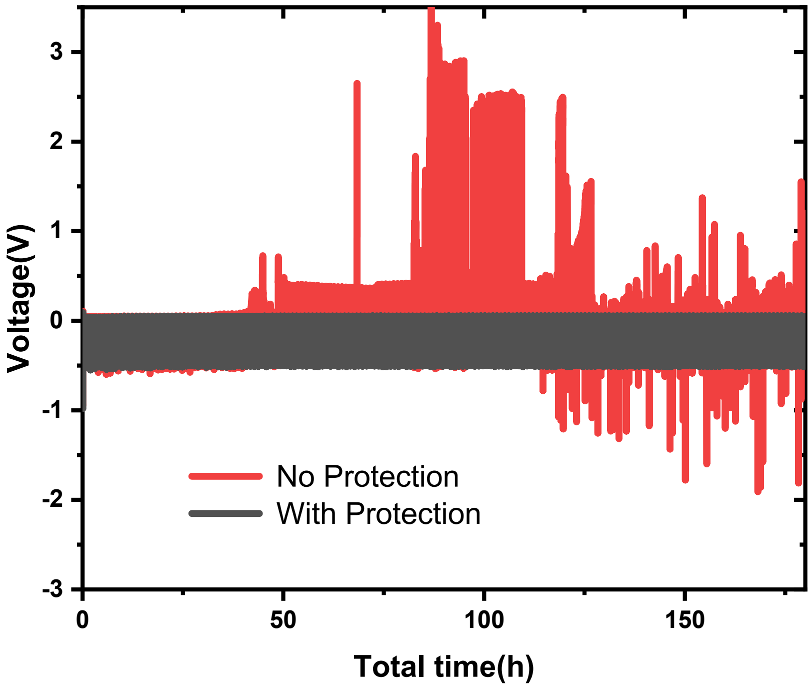

Fig. S9. The cycling of the coin cell with and without protection.

The cell with the protection ran much longer than the one without the protection.

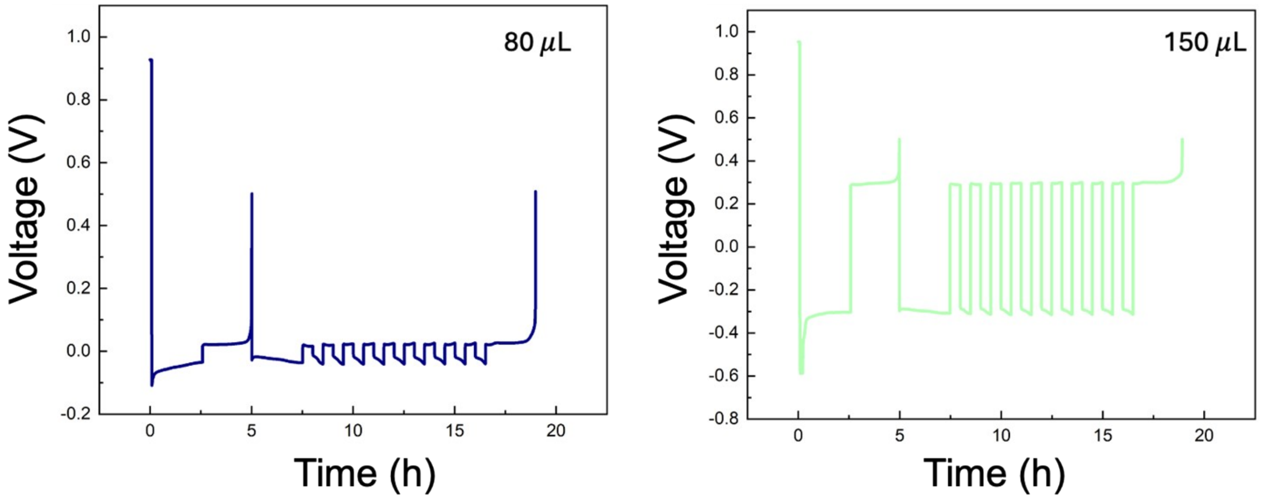

Fig. S10. The potential versus time curves for 80 and 150 μL under the galvanostatic charge-discharge protocol.

The Coulombic Efficiency obtained from here followed the trend of 40>80>150. (Average Coulombic Efficiency for 40μL :99.96%; 80 μL: 99.68%; 150 μL: 98.90%).

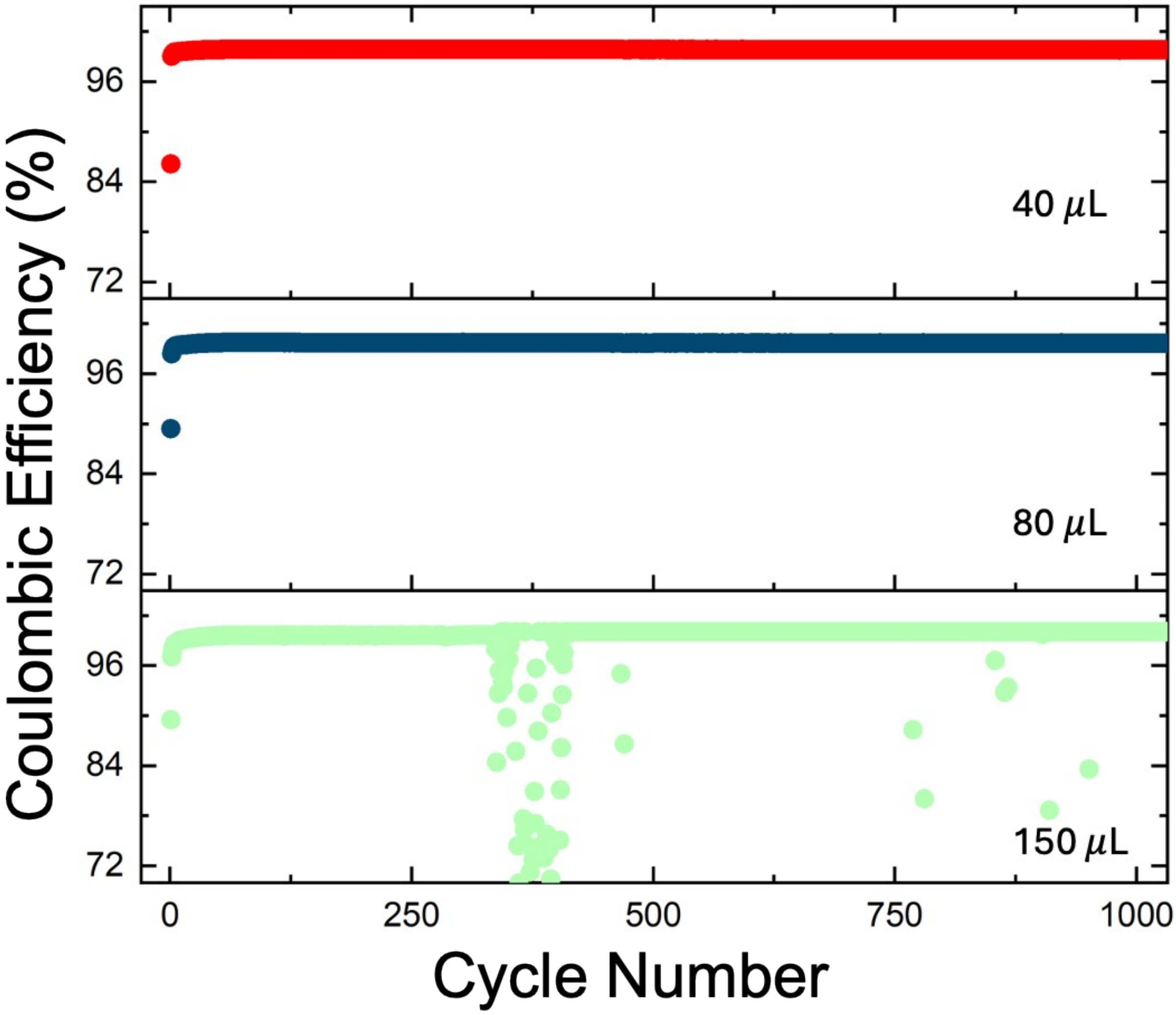

Fig. S11. The performance of Zn||Cu cells with different amounts of electrolyte added.

Not only was the performance of the lower electrolyte higher, but from the curve above we can also say that it lasted more cycles. (Average Coulombic Efficiency for 40µL :99.40%; 80 µL: 99.31%; 150 µL: 98.99%).

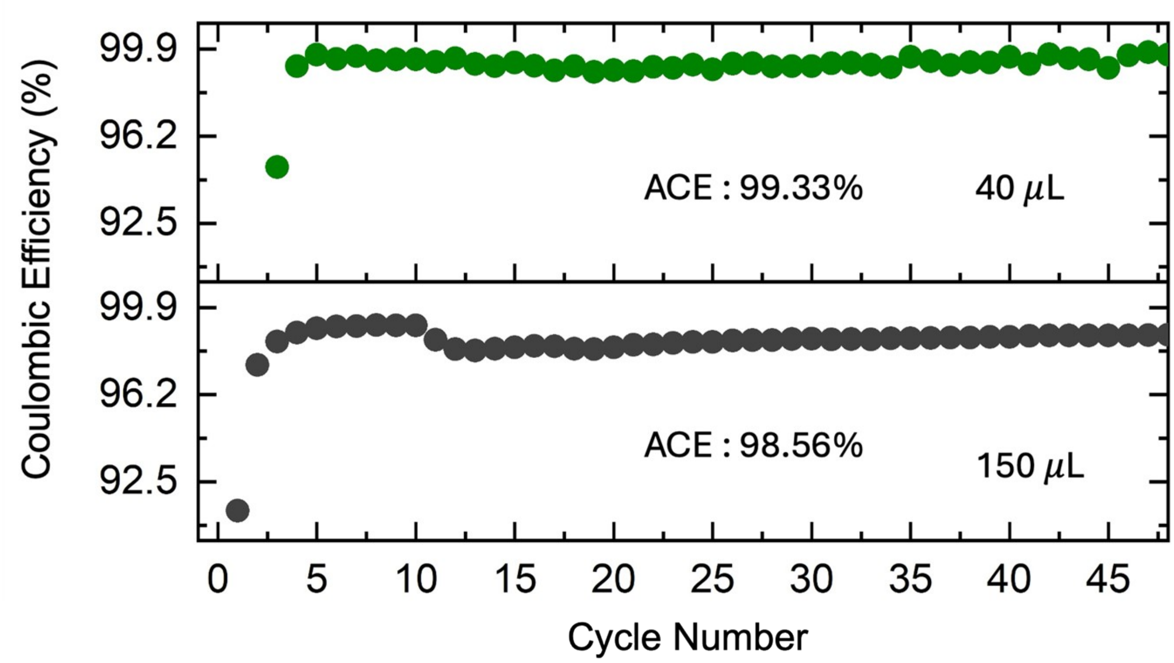

Fig. S12. The performance of Zn||Cu cells with $ZnCl_2$ as the salt with different amounts of electrolyte added.

Not only was the performance of the lower electrolyte higher, but from the curve above we can also say that it lasted more cycles. The ACE for both electrolytes amount can be shown.

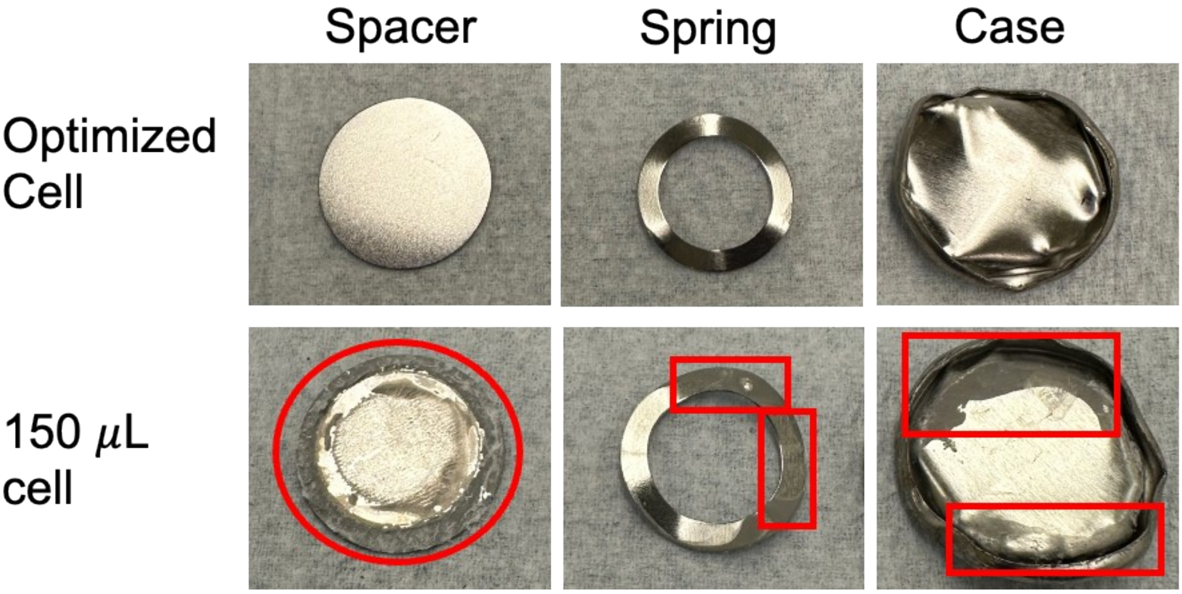

Fig. S13. The cell components (spacer, spring, and positive case) of Zn-Cu cells with an optimized cell and a 150 μL cell after 50 cycles.

The optimized cell shows no corrosion while the 150 μL cell components show corrosion which are showcased in red